ELSEVIER

Surface Science 365 (1996) 557–571

surface science

Study of the surface electronic structure of MgO bulk crystals and thin films

D. Ochs [a], W. Maus-Friedrichs [a,*], M. Brause [a], J. Günster [a], V. Kempter [a], V. Puchin [b], A. Shluger [b], L. Kantorovich [c,1]

[a] *Physikalisches Institut der Technischen Universität Clausthal, Leibnizstrasse 4, D-38678 Clausthal-Zellerfeld, Germany*
[b] *Institute of Chemical Physics, University of Latvia, Rainis Blvd. 19, Riga LV-1586, Latvia*
[c] *Physics Department, Keele University, Keele, Staffordshire, ST5 5BG, UK*

Received 2 January 1996; accepted for publication 20 March 1996

Abstract

The electronic structures of the surfaces of MgO single crystals, oxidized Mg polycrystals and oxidized Mg films grown by molecular beam epitaxy on Si(100) surfaces were studied using several techniques. These include metastable impact electron spectroscopy (MIES), ultraviolet photoelectron spectroscopy (UPS (He I)), and X-ray photoelectron spectroscopy (XPS). Spectra of oxidized Mg layers on Si(100) show additional features to those obtained for cleaved MgO crystals. These spectral features are attributed to dissociative adsorption of oxygen at bulk oxygen sites. Weak heating of the oxidized Mg layers removes these features and the electronic spectra for all three studied systems become similar. However, the experimental MIES and UPS spectra, both arising mainly from the ionization of the O 2p orbitals, have different structures. They are interpreted on the basis of ab initio Hartree–Fock and density functional calculations of the electronic structures of the ideal MgO(100) surface. It is shown, that the differences in the spectra can be understood by taking into account that UPS spectra reflect the density of electronic states within several surface layers, whereas MIES probes the surface states which are the most extended into the vacuum.

Keywords: Ab initio quantum chemical methods and calculations; Density functional calculations; Insulating films; Insulating surfaces; Magnesium oxides; Manganese; Metastable impact electron spectroscopy; Oxygen; Photoelectron spectroscopy; Silicon

1. Introduction

Geometric and electronic structures of the outermost surface layers determine most applications of insulating surfaces. However, our knowledge and understanding of the properties of these surfaces and especially of their electronic structures, are very limited. During the last few years, surface-sensitive spectroscopic techniques such as MIES and UPS have proved to be very useful in monitoring the development of the electronic structure of insulating films during their growth on metallic substrates [1–7]. It is our intention to apply these techniques in the future to study the details of surface morphology, adsorption of molecules and point defects at insulating surfaces. Theoretically, MIES should at present allow one to register one defective site among about 10^4 perfect surface sites. However, at these relatively small defect concentrations, the intensity of spectral features corresponding to defect electronic states in MIES spectra is very low. Therefore, differently prepared

* Corresponding author. Fax: +49 5323 723600; e-mail: wmf@physik.tu-clausthal.de

[1] On leave from the University of Latvia, Riga, Latvia.

PII S0039-6028(96)00706-6

surfaces (which can be later used as a reference for the study of induced surface defects) have to be studied and characterized first, which will be done in this paper.

MgO is widely used as a support for adsorption and growth of different materials, such as metals [8–12], semiconductors [13], superconductors [14] and optoelectronic devices [15]. It is also used as a catalyst for heterogeneous reactions [16]. It is resistant to damage by electrons of up to several keV impact energy and to damage by photon impact, and has a high temperature stability. Therefore it is instructive to study MgO surfaces prepared using different techniques as "reference" systems for further defect studies. The experimental study of insulators is often difficult due to a complicated cleaning procedure and charging up when employing electron spectroscopic techniques. We try to avoid this problem in two ways: (i) by using thin insulating films on metallic or semiconducting substrates, and (ii) by charge compensation using a simple electron source in the case of bulk MgO.

Freshly prepared (100) surfaces of MgO bulk samples and the surfaces of thin films produced by the oxidation of polycrystalline Mg surfaces and by the oxidation of Mg layers on Si(100) are studied using a combination of MIES and UPS (He I) for the analysis of the electronic surface properties, and by applying XPS for the estimation of layer thickness and for the analysis of the type of chemical bonding. Interpretation of the experimental MIES and UPS spectra is based on the theoretical surface densities of states. These are calculated by ab initio band structure methods for ideal MgO(100) surfaces.

2. Experimental techniques

The apparatus has been described in detail previously [17,18]. Briefly, it is equipped with a cold-cathode gas discharge source for the production of metastable He* $2^3S/2^1S$ ($E^* = 19.8/20.6$ eV) atoms with thermal kinetic energies and He I photons ($E^* = 21.2$ eV) as a source for UPS. The triplet-to-singlet ratio has been measured by He*–Ar impact as 7:1. He* 2^1S atoms are known to be very efficiently converted into He* 2^3S atoms in front of metallic and semiconducting surfaces [19–21]. An analogous conversion has also been observed for insulating surfaces, although its mechanism is not yet well understood. Nevertheless, only de-excitation from He* 2^3S is observable from the studied metallic, semiconducting and insulating surfaces. Metastable and photon contributions within the beam are separated by means of a time-of-flight technique combined with a double counter system which allows simultaneous MIES and UPS measurements. The angle of incidence of the probe beams is 45°; electrons emitted in the direction normal to the surface are analyzed. The simultaneous collection of an MIES/UPS spectrum takes about 1 min. MIES, UPS and XPS measurements are performed using a hemispherical analyzer (VSW HA100) with an energy resolution of 250 meV for MIES/UPS and 2.5 eV for XPS. The kinetic energies $E_{kin} = 21.2$ eV (UPS) and $E_{kin} = 19.8$ eV (MIES) displayed in the spectra correspond to electrons emitted from the Fermi level of the substrate. These are the largest possible energies of the electrons achieved in the experiments. The low-energy onset of the electron spectra directly reflects the surface work-function, therefore its variation with exposure directly gives the exposure dependence of the work function. XPS spectra are displayed as a function of the binding energy. Additionally, the apparatus is equipped with the standard LEED and AES tools.

MIES and UPS experiments on the Mg films grown on Si(100) and those on the polycrystalline Mg surface were performed biasing the target by 50 eV, which has been shown to have almost no influence on the spectral features. However, the MgO(100) single crystal surfaces were not biased during MIES and UPS measurements. The spectra are therefore cut on the low-energy side, reflecting the difference between the target and analyzer work functions. Due to the fact that all important spectral features are visible, no further attempts were made to improve the measurements.

Mg layers were produced by evaporating Mg from a commercial Knudsen cell on the Si(100) surfaces. The evaporation is done at a cell temperature of 220°C thus producing about half a monolayer of Mg per minute. Polycrystalline Mg

surfaces were cleaned by sputtering with Ar^+ ions (5 kV with 10 μA cm^{-2}) for 2–3 h followed by subsequent annealing to about 600 K for about 2 min. This cycle was repeated several times. MgO(100) crystals were cleaned by sputtering with Ar^+ ions (4 kV with 5 μA cm^{-2}) for 2–3 h with subsequent annealing to 1300 K for 3 min. Surface cleanliness was monitored by MIES and XPS. Oxygen was offered by an UHV valve, the oxygen partial pressure was obtained by means of a quadrupole mass spectrometer. The thickness of the Mg layer on Si(100) is estimated on the basis of the ratio of Si 2p and Mg 2p XPS peaks. This ratio decreases exponentially as a function of layer thickness.

The base pressure of the apparatus was 7×10^{-11} Torr; during the evaporation of Mg the pressure was 3×10^{-10} Torr.

In MIES experiment, about 10^9 He* per mm^2 were scattered per second at the target, and the hemispherical analyzer counted the electrons emitted from an area of about 1 mm^2. If we assume unity de-excitation probability and an electron analyzer transmission probability of 0.1, the estimated sensitivity of MIES to randomly distributed surface defect sites is 10^{-4}, providing the defects contribute to the electronic states within the optical band-gap of the reference system. The sensitivity to defect-induced changes within the valence band emission of the reference system is much lower.

All measurements were performed at room temperature. For the oxidation of polycrystalline Mg and Mg layers on Si(100) (typically less than 3 nm thick) the results are presented as a function of the exposure to oxygen. For these systems, no charging problems arise. MgO(100) bulk crystals charge up during MIES and UPS. To compensate this surface charge, a simple electron source was introduced near the target. A tungsten filament was heated and a potential difference between filament and target of +2 V was applied. Using this simple equipment, no shift of the electron distribution during the energy analysis was observed.

Below about 10 eV both the UPS and the MIES spectra appear to be dominated by secondary electrons; this part of the spectra will not be discussed in the following.

3. Methods of interpretation of MIES and UPS spectra

Experimental angle-resolved photoelectron spectra (He I and He II) from MgO(100) have been reported in Ref. [22]. It was demonstrated by a comparison with band-structure calculations that the observed double-peak structure in the UPS (He I) valence-band spectra essentially reflects the valence-band density of states (DOS). This conclusion was confirmed by more recent band-structure results and photoelectron spectra [23]. For the geometry chosen here, the UPS (He I) spectra show the same structure. Therefore, we assume in our analysis that the UPS (He I) spectra can be considered as reflecting the valence-band DOS.

The interpretation of the results of MIES experiments is based on the model introduced by Niehaus et al. [24,25] and will be briefly discussed below.

The interaction of metastable He* atoms with the surface can occur via the following processes [26,28].

Auger capture (AC) takes place for metals and semiconductors with work functions larger than 3.5 eV. In this process, in the first stage, the He 2s electron is transferred into an unoccupied surface state by resonance transfer (RT), whereas in the second stage, a surface electron fills the He 1s hole while a second surface electron is emitted, carrying the excess energy.

Auger de-excitation (AD) takes place when no unoccupied surface states are in resonance with the He 2s state. This is usually the case for metals with work functions below 3 eV and in general for insulators, in particular also in the present case. A surface electron fills the He 1s hole while the He 2s electron is emitted carrying the excess energy. In contrast to UPS, the band structure of the bulk is of no concern because the emitted electron is represented by a free-electron state located at the He probe atom.

For work functions below about 2.2 eV, the RT of a surface electron to the He* 2s can take place, producing a negative excited He ion in front of the surface prior to de-excitation. This ion decays by a fast intra-atomic Auger process called autodetachment (AU), where one of the He 2s electrons

fills the He 1s hole while the second He 2s electron is emitted.

Numerical simulation of the spectra allows one establish the relative importance of different interaction processes. Within the numerical simulation each of the described projectile states is represented by its time-dependent occupation, which can be changed along the projectile's trajectory by the competition of the described transition processes. A set of coupled rate equations is solved numerically for every involved state along the trajectory of the projectile. This simulation procedure was successfully applied to He^+ and He* collisions with clean and alkali-covered metal surfaces [27], and LiF layers [5].

We confine ourselves to situations where the electronic interaction between the He metastable atom and the surface is only due to AD involving O 2p electrons. This is fulfilled as soon as the resonant transfer of the He 2s electron is inhibited due to the insulator band-gap.

The differential transition probability for AD (g_{AD}) is approximately given by the overlap of the relevant wave functions of the probe atom and of the surface [24,25,28], and can be written as

$$g_{AD}(z,E_b)=An(E_b)\exp(-z\gamma), \tag{1}$$

$$\gamma=2\left(\frac{1}{\sqrt{2E_b}}+\frac{1}{\sqrt{2E(z)}}\right)^{-1}, \tag{2}$$

where E_b is the binding energy of the surface electron, $n(E_b)$ is the surface density of states (SDOS) and $E(z)$ is the He 1s electron binding energy, i.e. the corresponding ionization energy. In Eq. (1) we assume that the SDOS does not depend on the distance z from the surface along the trajectory of projectile. The AD rate in Eq. (1) is factorized in such a way that z appears only in the exponential function which approximates the squared overlap of the projectile atomic orbital with the surface wave-function. The exponential parameter γ depends on the electron binding energy reflecting in average the asymptotic behavior of the surface wave-function. In fact, the surface wave-functions die away into the vacuum in a more complicated way because there is a prefactor to the exponentials. Different projections of the density of states will be used instead of $n(E_b)$ in the expression for the electronic transition rate in order to account for this point.

The trajectory of the projectile is defined by its interaction with the surface. In general, this interaction is different for the initial (He* $1s2s;^3S$), and the final (He^0 $1s^2;^1S$), states of the atom. It is approximated by a superposition of a repulsive potential, based on the He–oxygen interaction,

$$V_r(z)=A_r\exp(-\alpha_r z), \tag{3}$$

with $A_r=57.92$ au and $\alpha_r=1.71$ au^{-1}, the interaction via the Madelung potential

$$V_m(z)=-\frac{4\sqrt{2}qZ_{eff}(z)}{a}\exp\left(-\frac{\pi\sqrt{2}z}{a}\right), \tag{4}$$

where $q=2$ and $a=3.98$ au are the ionic charge and the lattice parameter, respectively, $Z_{eff}(z)$ is the distance-dependent effective charge, and the effective image potential [29,30]

$$V(z)=\frac{\epsilon-1}{\epsilon+1}\frac{Z_{eff}^2(z)}{4(z-z_{im})}\left(1-\exp\left(-\alpha_{cut}(z-z_{im})\right)\right). \tag{5}$$

Here α_{cut} is the cut-off radius of the image interaction, and z_{im} is the position of the image plane ($z_{im}=2.5$ au in front of the surface). Z_{eff} is state-dependent and was modeled as described in Refs. [24,25]. For MgO we use the static value of the dielectric constant, $\epsilon=9.65$ [31].

Under the present conditions, when the projectile moves with small (thermal) kinetic energies, the electron emission due to AD of He* occurs on the incoming part of the trajectory at comparatively large distances ($z\approx 2.5$ Å), and the transition energy is not much influenced by the actual interaction potentials in initial and final states. Therefore the simulated energy spectra reflect the SDOS used as an input in a rather direct way.

In order to find the SDOS required for the calculation of the transition rates, two ab initio band-structure calculation techniques were employed. Ab initio methods have been used extensively for the calculation of electronic band-structure and atomic relaxation of both ideal (100) and defective MgO surfaces [32–41]. However, until now not much attention has been paid to calculations of the surface density of states, which

are relevant to surface-sensitive electron spectroscopic methods such as MIES. In this study, the electronic densities of states have been calculated by the CRYSTAL and CASTEP computer codes.

The CRYSTAL code [34] is based on the Hartree–Fock (HF) approximation. Crystalline orbitals (one-electron wave functions) are treated as linear combinations of Bloch functions constructed from a basis set of atomic orbitals. The non-local electron exchange interaction is treated exactly and electron correlation is neglected. Detailed descriptions of the method and computer code have been published elsewhere [32]. In this work, we employed the optimized basis set for Mg and O ions [35] which was successfully used for the simulation of a CO molecule adsorption on the MgO(001) surface [36].

The atomic functions are localized and therefore well-suited to the study of the density of states inside the crystal and within the surface layers. The total density of states (ρ) can be separated into atomic (ρ_x) and further into the atomic orbital contributions (ρ_v).

$$\rho(\epsilon)=\sum_x \rho_x(\epsilon), \tag{6}$$

$$\rho_x(\epsilon)=\sum_{v\in x} \rho_v(\epsilon), \tag{7}$$

$$\rho_v(\epsilon)=\frac{2}{V_B}\sum_j \sum_\mu \int_{BZ} \mathrm{d}k\, S_{v\mu}(k)c_{vj}(k)c^*_{\mu j}(k)\delta[\epsilon-\epsilon_j(k)], \tag{8}$$

where V_B is the volume of the Brillouin zone, indices v and μ denote atomic orbitals or corresponding Bloch functions, j are crystalline orbitals or electron bands, $\boldsymbol{k}$ is the vector in the Brillouin zone (BZ), $\epsilon_j(\boldsymbol{k})$ and $c_{vj}(\boldsymbol{k})$ are the one-electron energies (Hartree–Fock eigenvalues) and the wave-functions (Hartree–Fock eigenvectors) in the atomic orbital representation, and $S_{v\mu}(\boldsymbol{k})$ is the Fourier transform of the atomic orbital overlap matrix. ρ_x and ρ_v are also called the projected density of states to the atoms, and atomic orbitals, respectively.

For the calculation of the SDOS we have also used the CASTEP code [42]. This code is based on the local density approximation (LDA) and uses core pseudopotentials. Details of the method and the computational procedure can be found in Refs. [42–44]. The total energy of the crystal is minimized with respect to coefficients in the plane-wave expansion of the crystalline orbitals. Exchange and correlation potentials are calculated approximately as a local functional of electron density. Since the basis of plane waves is not associated with atoms and atomic orbitals, the density of states projected on atoms can be calculated by numerical integration of the electron density in the direct space within a sphere V_x centered on the atom x and having a radius equal to the atomic or ionic radius

$$\rho_x(\epsilon)=\frac{2}{V_B}\sum_j \int_{BZ} \mathrm{d}k \int \mathrm{d}r|\psi_j(k,r)|^2\delta[\epsilon-\epsilon_j(k)]. \tag{9}$$

Eq. (1) is based on the assumption, that the crystal wave-functions $\psi_j(\boldsymbol{k},\boldsymbol{r})$ decay exponentially out of the surface. To check this, one can calculate the so-called plane projected density of states above the surface. It is defined as an integral over a plane lying parallel to the surface of the crystal at a distance z

$$\rho(\epsilon,z)=\frac{2}{V_B}\sum_j \int_{BZ} \mathrm{d}k \int \mathrm{d}x\,\mathrm{d}y\,|\psi_j(k,r)|^2\delta[\epsilon-\epsilon_j(k)]. \tag{10}$$

For large z, this density of states should behave in average as $\exp(-2\sqrt{2\epsilon}z)$. We have checked that this is indeed the case for the CASTEP calculations in the region of $z\lesssim 4$ Å. In the case of CRYSTAL calculations, we have checked directly the asymptotic of the wave functions. We found exponential behavior for distances $z\lesssim 5$ Å. Due to the fact that metastable He* atoms interact with surfaces predominantly at distances between 2 and 3 Å, the accuracy of our calculations is sufficient for our purpose.

A slab of six atomic layers has been used to simulate the MgO(100) surface using both techniques. The relaxation of the top surface layer has been taken into account. Displacements of ions, obtained by CRYSTAL and CASTEP methods, are essentially the same [35,43]. In the present study we have chosen the values 0.022 Å for O (outwards) and −0.018 Å for Mg (inwards).

In order to compare experimental electron spectra with the calculated density of states, broadening of the spectra due to different physical effects should be accounted for. In the case of the MgO crystal, which has a relatively narrow valence band and large band gaps, the theory of the UPS core line broadening has been applied also to the valence band electron spectra. Core lines have a Gaussian shape due to the phonon broadening effects. The lifetime broadening, which has a characteristic Lorenzian shape, is negligible. The Gaussian width (ΔE) at the half maximum can be estimated from the hole relaxation energy (E_R) and optical phonon frequency $\hbar\omega_{LO}$ [45,46]

$$\Delta E = 2.35\sqrt{\hbar\omega_{LO}E_R \coth\left(\frac{\hbar\omega_{LO}}{2kT}\right)}. \quad (11)$$

The relaxation energy for the one-centre valence hole in MgO has been calculated to be 2.4 eV [47]. Using this value of E_R and $\hbar\omega_{LO} = 68.7$ meV [48], one obtains $\Delta E = 1.0$ eV at room temperature. For the valence band, the electron spectra can be compared to the theoretical results by convolution of the calculated density of states with this Gaussian

$$n(\epsilon) = \frac{1}{\Delta E}\sqrt{\frac{2}{\pi}}\int d\epsilon'\, \rho(\epsilon') \exp\left(-\frac{2(\epsilon-\epsilon')^2}{\Delta E^2}\right). \quad (12)$$

It is interesting to note that value of $\Delta E = 1.0$ eV estimated above gives the best agreement between experimental UPS spectrum and calculated density of states of the O 2p valence band. Therefore, we also used the same expression for $n(\epsilon)$ in Eq. (1) for the transition probability in the simulations of MIES. It is worth noting that the phonon frequencies and the hole relaxation energy at the surface may differ from those in the bulk. However, to our knowledge, the corresponding data is absent in the literature and we have used the same value for ΔE.

4. Results

4.1. MgO bulk

The MIES and UPS (He I) spectra of the MgO(100) single crystal surface are presented in Fig. 1. The Fermi level (denoted by E_F) has been determined using a metal target instead of the insulator in the same position, which defines its position. All binding energies refer to E_F. They agree well with those obtained for the corresponding features seen for the MgO films (see Fig. 8).

The UPS spectrum has two peaks at binding energies $E_B = 5.6$ and 8.3 eV, and is similar to previously published UPS spectra of MgO(100) [22]. The UPS peak structure is similar to that reported previously [22], although the double-peak structure appears to be somewhat more pronounced. It is attributed to emission from the O 2p valence band [22]. Comparable spectra are found for other metal oxides, for example Al_2O_3 [49]. For the following discussion of the results, the two peaks will be denoted as O $2p_{5.6}$ and O $2p_{8.3}$. As one can see in Fig. 1, MIES shows only the peak at $E_B = 5.6$ eV, and no indication of the peak at 8.3 eV. No MIES results are available from the literature for a comparison of our MIES result.

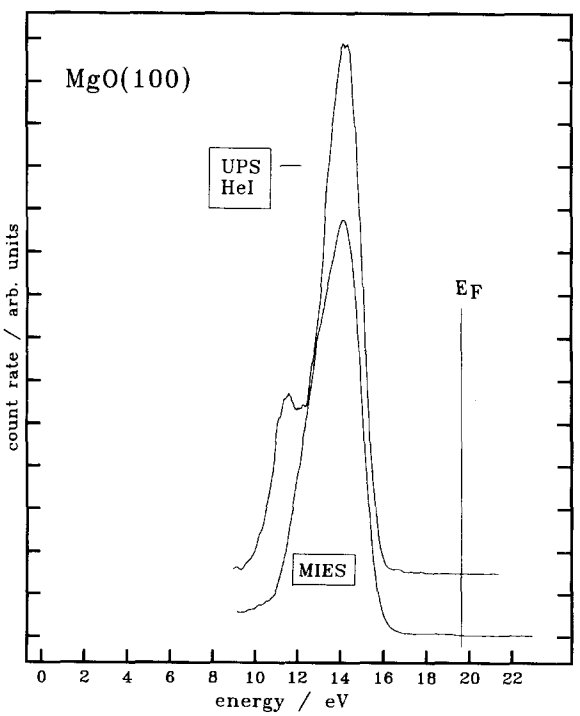

Fig. 1. MIES and UPS (He I) spectra from a clean MgO(100) surface. The UPS spectrum has been shifted by 1.4 eV to lower energies in order to align the Fermi levels E_F.

According to the results of recent calculations [43], even for the surface containing steps and kinks, there are no surface states in resonance with the impinging He 2s electron. Therefore no resonance transfer can occur and the metastable atom–surface interaction most probably takes place exclusively via Auger de-excitation. As mentioned above, during the measurement of MIES and UPS spectra the target was not biased. For this reason, the spectra below $E_{kin}=9$ eV may be influenced by slow electrons from the other apparatus equipment. For clarity, spectra are therefore only shown for $E_{kin} \geq 9$ eV.

The XPS spectrum of the MgO bulk in Fig. 2 shows no contributions from metallic Mg, which would be indicative for an improper cleaning procedure. The main Mg $KL_{2,3}L_{2,3}$ Auger peak is found at a binding energy of 316 ± 0.3 eV, and no other Mg contributions were observed. In particular, the feature seen around 270 eV is part of the Mg KLL Auger emission and has been reported previously [50]. Our spectrum, as far as the KLL emission is concerned, agrees well with that reported in Ref. [50]. No contributions arising from impurities or contaminations were found. Carbon monoxide adsorbed on top of the surface, which produces an additional peak belonging to C 1s at $E_B=295$ eV, was removed by mild heating. During the oxidation of polycrystalline Mg crystals, a binding energy for the Mg $KL_{2,3}L_{2,3}$ Auger peak of 308 eV was found [51]. The fact, that we found the corresponding peak at about $E_B=316$ eV indicates a surface charge-up, resulting in a peak shift of about 8 eV.

4.2. Oxidation of Mg(poly)

The UPS results obtained during the oxidation of a polycrystalline Mg surface are presented in Fig. 3. The bottom spectrum shows the result for the pure Mg(poly) surface. It exhibits a low counting rate due to a very small cross-section for ionization of Mg 3s states by He I photons [52]. The oxygen exposure increases by 10 L ($1\ L=10^{-6}$ Torr · s) per spectrum. At first a peak at

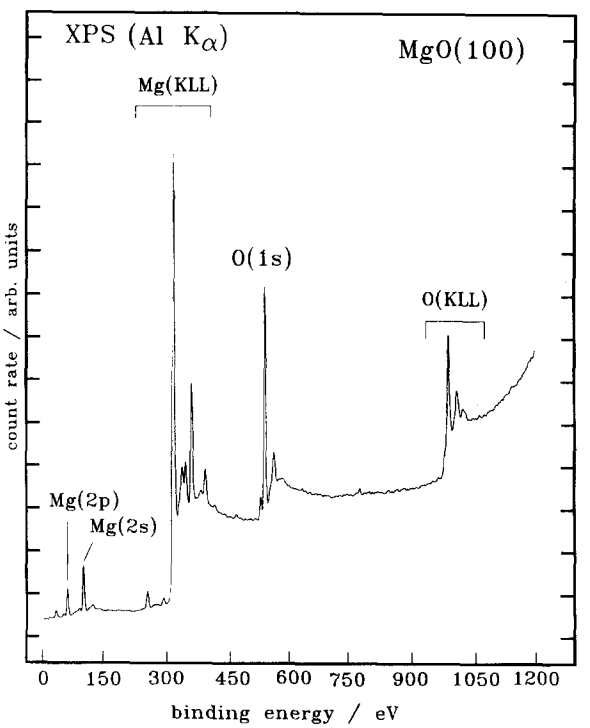

Fig. 2. XPS spectrum from a clean MgO(100) surface.

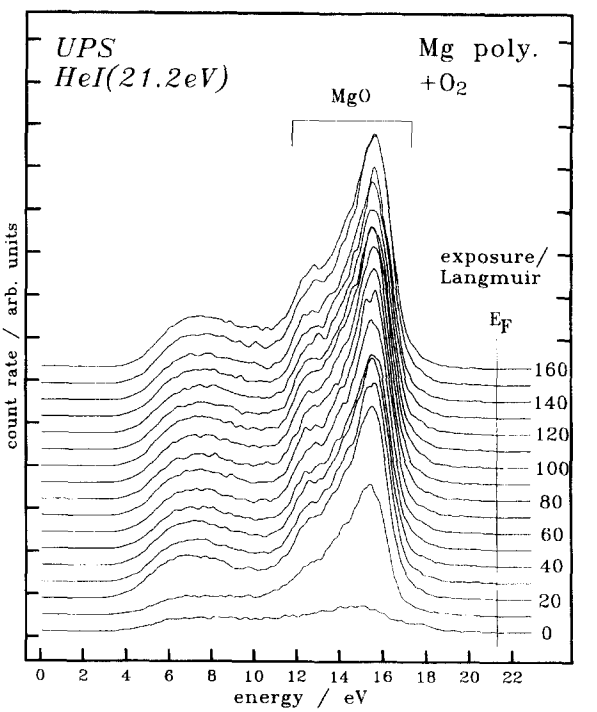

Fig. 3. UPS spectra from a polycrystalline Mg surface as a function of oxygen exposure.

$E_B = 5.7$ eV develops, and a pronounced shoulder at 8.5 eV becomes visible for oxygen exposures beyond 20 L. Saturation is reached for an oxygen exposure of 80 L. The main spectral features at saturation are almost identical to those obtained for the MgO(100) bulk crystal. However, some additional contributions with kinetic energies corresponding to states beyond the valence-band maximum (i.e. in the band gap) occur.

The MIES spectra for different stages of oxidation of the polycrystalline Mg surface with the oxygen exposure increasing by 10 L per spectrum are shown in Fig. 4. The bottom spectrum corresponds to the pure Mg(poly) surface. The theoretical maximum kinetic energy for an electron produced by AC amounts to about 18 eV for He*, for a surface work-function of 3.5 eV. The bottom MIES spectrum is therefore almost completely produced by AC, with only small contributions from AD visible beyond $E_{kin} = 18$ eV. As the oxygen exposure increases, the peak at $E_B = 5.6$ eV develops intensely and additionally some small contribution can be seen at about $E_B = 8$ eV. The peak at 5.6 eV has the same nature as O $2p_{5.6}$ observed for the bulk. Beyond an oxygen exposure of 20 L, all the contributions to the MIES spectra are produced by AD. RT is inhibited due to the development of the insulator band-gap, and thus the AC process can no longer occur.

4.3. Oxidation of Mg films on Si(100)

Mg films with thicknesses greater than 100 Å were grown on clean Si(100) surfaces. The UPS spectra measured during the oxidation of these Mg films are presented in Fig. 5. These spectra are representative for Mg films with thicknesses greater than 20 Å. The bottom spectrum corresponds to the pure Mg film and is very similar to the result for the pure Mg(poly) surface (see Fig. 3). The exposure increases by 1 L per spectrum. Again the double peak corresponding to O 2p ionization at $E_B = 8.3$ eV and 5.8 eV develops. The spectrum saturates at an oxygen exposure of 20 L. Besides

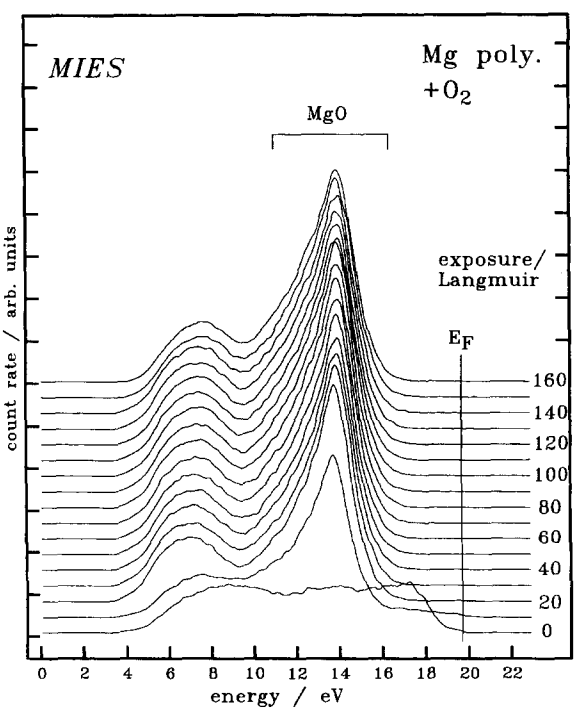

Fig. 4. MIES spectra from a polycrystalline Mg surface as a function of oxygen exposure.

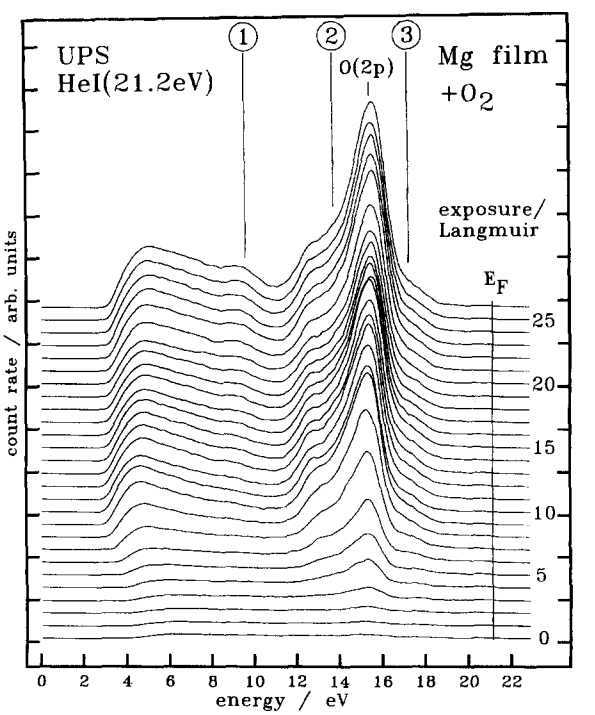

Fig. 5. UPS spectra from an Mg film (>100 Å) on Si(100) as a function of oxygen exposure.

the characteristic peaks corresponding to O $2p_{5.6}$ and O $2p_{8.3}$, it has additional shoulders at $E_B \approx 4.2$ eV (marked "3") and $E_B \approx 8.0$ eV (marked "2") and an additional peak at $E_B = 11.7$ eV (marked "1"). These additional features are not seen when MgO molecules are evaporated onto Si(111) [53].

Fig. 6 shows the MIES results for the oxidation of the same Mg layer. Besides the prominent broad O 2p peak at $E_B = 5.6$ eV, which is similar to O $2p_{5.6}$ observed for MgO bulk and oxidized Mg(poly) surfaces, an additional peak at $E_B = 11.3$ eV (marked "1") and an indication of a shoulder in the range of $E_B = 4$ eV (marked "3") also develop as in the UPS spectra in Fig. 5. Furthermore, the intensity in the region of O $2p_{8.3}$ appears much stronger than for the previous systems (MgO(100) and O_2/Mg(poly)), which is attributed to additional emission corresponding to the peak marked "2" in Fig. 5.

In the oxygen-exposure range 3–10 L, there is another spectral structure developing just below

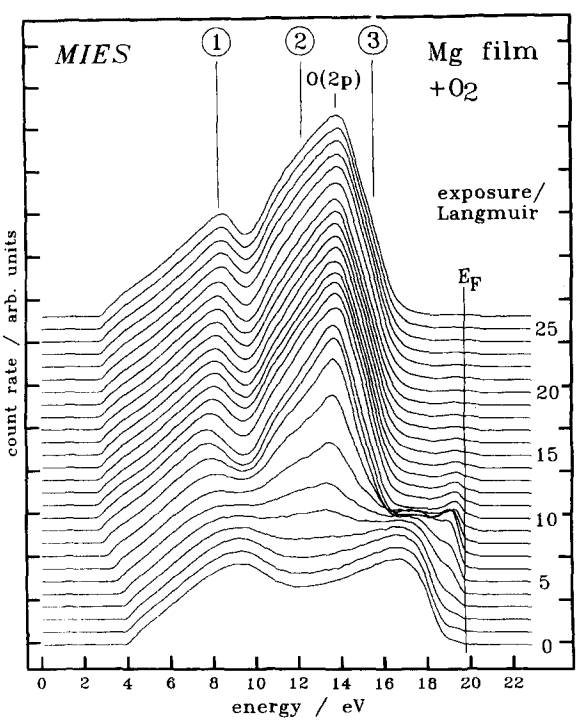

Fig. 6. MIES spectra from an Mg film (>100 Å) on Si(100) as a function of oxygen exposure.

E_F in the range $0 \leq E_B \leq 2$ eV. Similar spectral features were also found during the adsorption of alkali atoms on metals and semiconductors [1,2]. They were identified as being due to the autodetachment (AU) of $(He^-)^*$. Although this additional resonance transfer normally occurs for work functions below 2.2 eV, we cannot exclude that the observed feature is also due to AU of $(He^-)^*$. Its intensity sensitively depends on the surface work-function and the electron density below E_F. It decreases rapidly with forthgoing oxidation, which consumes the free electrons below E_F for the binding and the dissociation of oxygen. A similar behavior has been found for the oxidation of Li and Na films on W(110) [1].

The XPS spectra for the O 1s peak and the Mg $KL_{2,3}L_{2,3}$ peak during the oxidation of the Mg layer are shown in Fig. 7a and b, respectively. The oxygen peak at $E_B = 533.7 \pm 0.3$ eV corresponds to oxygen atoms incorporated in the MgO crystal. It increases in intensity without any peak shift, and reaches its saturation for an oxygen exposure of about 20 L. The bottom spectrum of Fig. 7b shows the result for the clean Mg layer. It is dominated by the prominent $KL_{2,3}L_{2,3}$ peak at $E_B = 303.3 \pm 0.3$ eV and a corresponding bulk plasmon loss peak ($\Delta E = 10.9$ eV) which has previously been observed in Ref. [51]. With forthgoing oxidation the plasmon loss peak decreases and a second Mg $KL_{2,3}L_{2,3}$ peak corresponding to Mg^{2+} incorporated in a MgO complex develops at $E_B = 308.3 \pm 0.3$ eV. A similar development of the second peak with a distance of 5.0 eV to the Mg peak, corresponding to the metallic phase, has also been reported for polycrystalline Mg layers in Ref. [51]. Even for the saturation oxygen coverage of 20 L the original Mg peak at $E_B = 303.4$ eV still remains visible. As has been estimated in Ref. [50], the thickness of the oxide layer on polycrystalline Mg at room temperature is about 7 ± 3 Å, and therefore it is not surprising that the contribution from the metallic Mg can also remain in our experiment. No additional oxygen-induced peaks appear at other binding energies.

The UPS and MIES spectra for the MgO(100) and oxygen-saturated Mg(poly) surfaces, as well as for the oxygen-saturated Mg film and for the same oxidized Mg film after weak heating to 800

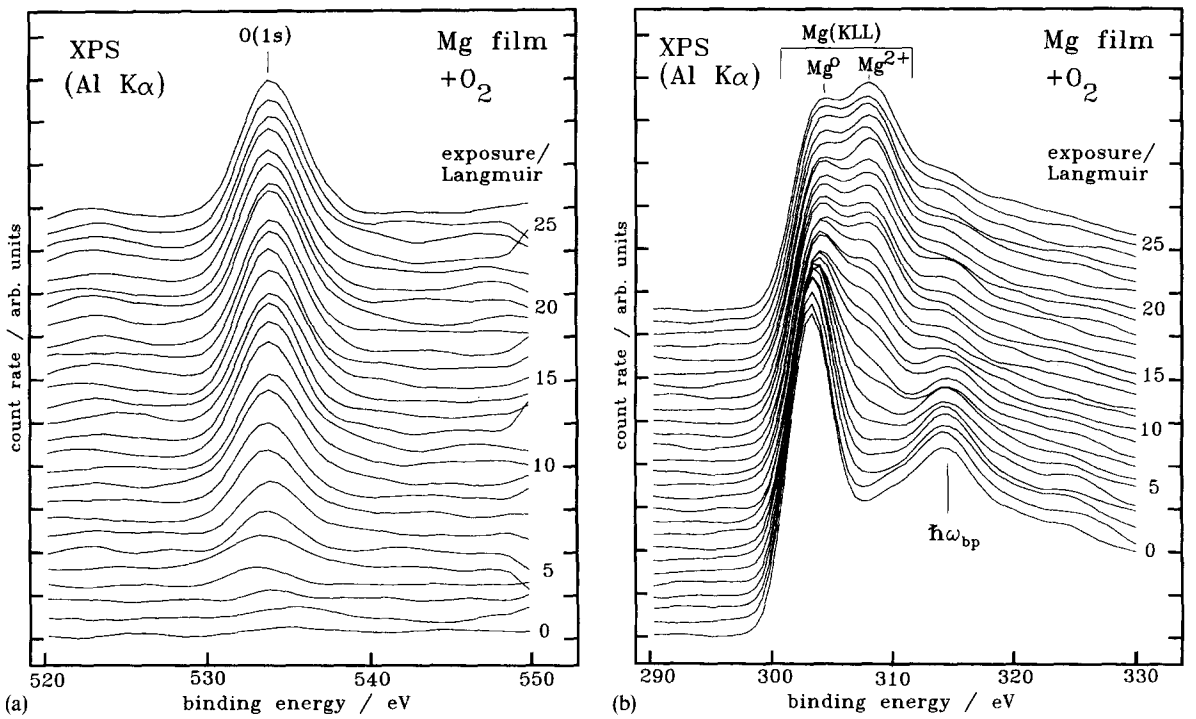

Fig. 7. XPS spectra from an Mg film on Si(100) as a function of oxygen exposure. (a) Oxygen O 1s peak and (b) main Mg $KL_{2,3}L_{2,3}$ peak.

K, are presented in Fig. 8. As can be seen, after the heating procedure the O 2p UPS and MIES valence band-structure of the Mg film become very similar to that of the MgO(100) surface, as well as to that for MgO/Si(111) [53]. Again beyond the valence band maximum, within the insulator band-gap, some contributions seem to appear which are not observed on the MgO(100) single crystal. These structures can be attributed to the electronic states produced by rough surfaces or by intrinsic defects [43]. As mentioned above, the spectra are dominated by secondary electrons below energies of about 7 eV. These features will not be discussed.

4.4. Results of calculations

To rationalize the experimental UPS and MIES spectra discussed above, the total density of electronic states, as well as different projections of SDOS, were calculated for the ideal MgO(100) surface. For comparison, we first calculated the total density of states (DOS) in the O 2p valence band of MgO crystal using both CRYSTAL (HF) and CASTEP (LDA) codes. The results presented in Fig. 9 demonstrate a good agreement of both techniques and are in agreement with previous results of LCAO calculations [54]. The energy difference between the two peaks obtained by the HF method is 3.05 eV, and their relative intensity is 0.58. The LDA method gives 3.10 eV for the peak distance and 0.62 for their relative height. For the comparison of theoretical and experimental results the UPS spectrum for the clean MgO(100) surface from Fig. 1 is also displayed in Fig. 9, but shifted in such a manner that the dominant maxima fit together. The UPS spectra should reflect the sum of contributions from the DOS of surface and bulk layers. The comparison between UPS data and calculated DOS (given in Fig. 9) generally shows a good agreement of both the spectral shape and the relative peak distance. For the oxidized films, some additional contributions are observed in the experimental spectra, pointing to the presence of some surface defects (see below).

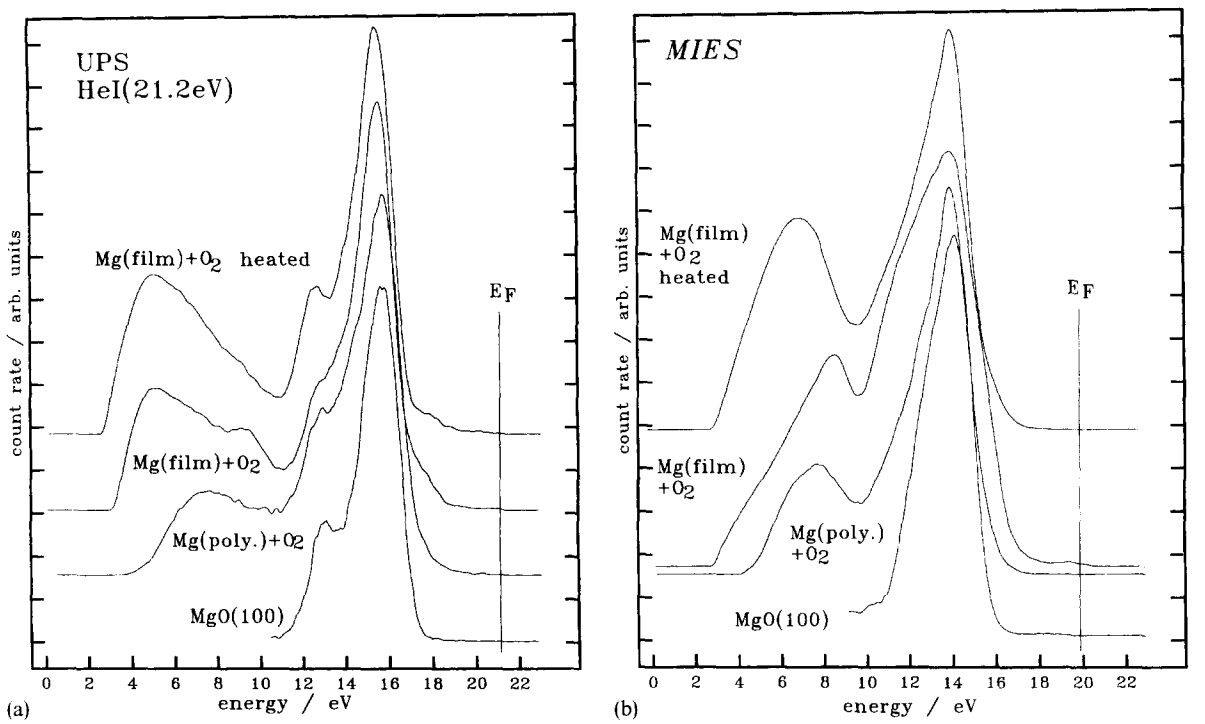

Fig. 8. (a) UPS spectra and (b) MIES spectra of MgO(100), oxidized Mg(poly), oxidized Mg film and heated oxidized Mg film (see text).

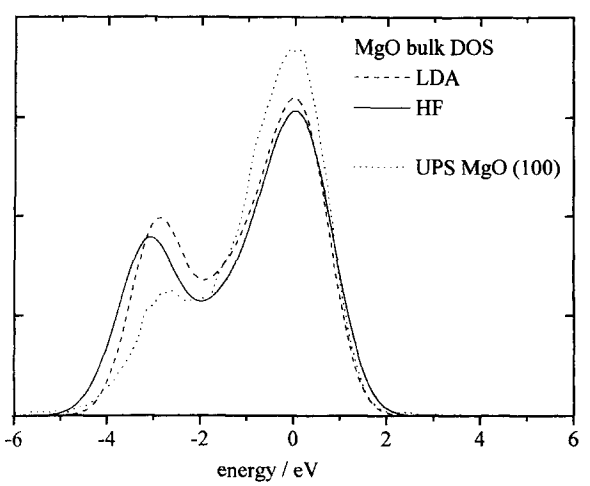

Fig. 9. Density of states for bulk MgO calculated by CRYSTAL (HF) and CASTEP (LDA) code and the experimental UPS spectrum for MgO(100) from Fig. 1. The curves are shifted on the energy scale so that the main peak is positioned at the zero energy.

Projected densities of states (PDOS) on the O ions in different layers of MgO(100) slab calculated by the CRYSTAL method are shown in Fig. 10 with and without surface relaxation. The PDOS in the third layer is identical to the bulk DOS (BDOS). The second-layer PDOS shows a slight increase of the left (higher binding energy) peak relative to the bulk DOS. In the surface layer PDOS, this peak is much smaller than for the bulk DOS and the whole spectrum is shifted to lower binding energies by about 1 eV. Comparison of Fig. 10a and b shows that the small lattice relaxation of about 1% of the lattice parameter induces noticeable changes in the projected density of states, decreasing the ratio of the peak intensities from 0.38 to 0.26.

We should accentuate that parallel p_x (O $2p_{\parallel}$) and perpendicular p_z (O $2p_{\perp}$) p-orbital contributions of the surface oxygen to the density of states presented in Fig. 9 differ dramatically. While O $2p_{\parallel}$ displays a two-peak structure similar to the bulk DOS, O $2p_{\perp}$ shows only one peak at a

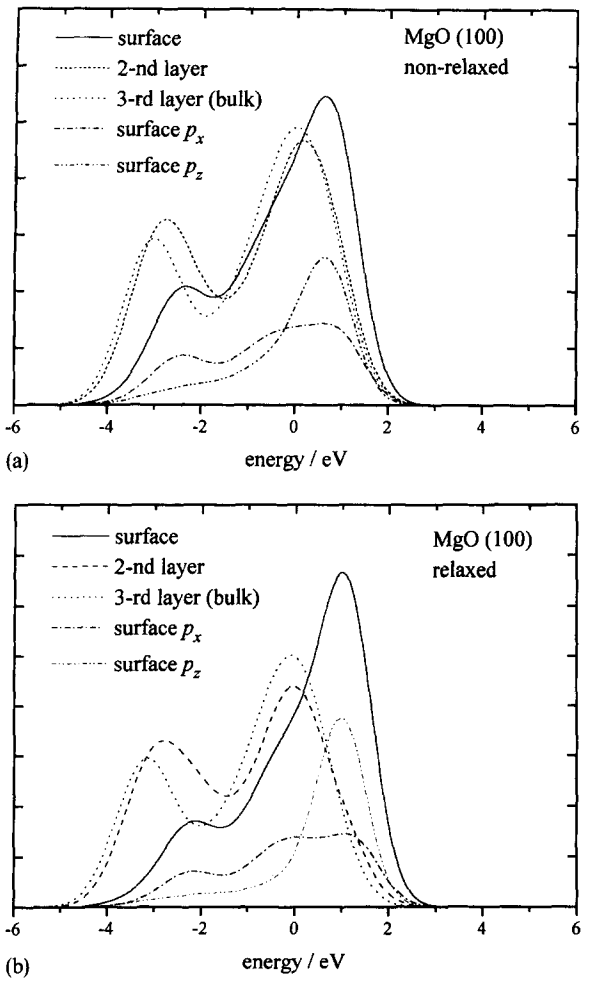

Fig. 10. Calculated DOS for the MgO slab (see text): PDOS of the top layer (surface), of the second and third layers (second-layer and third-layer (bulk)), DOS of the top layer projected both on the p_x oxygen orbital parallel to the surface (surface p_x) and the p_z oxygen orbital normal to the surface (surface p_z) (a) without and (b) with relaxation of surface atoms. The energy shift is the same as described in Fig. 9.

smaller binding energy. The width of the O $2p_\perp$ peak decreases if the surface relaxation is taken into account.

In Fig. 11 we compare the experimental MIES spectrum for the MgO(100) single crystal with the following calculated DOS: the p_z DOS and the top-layer PDOS from Fig. 10 calculated by the CRYSTAL code (HF), and the top-layer PDOS calculated using the CASTEP code (LDA) (Eq. (9)). For this purpose, the calculated densities

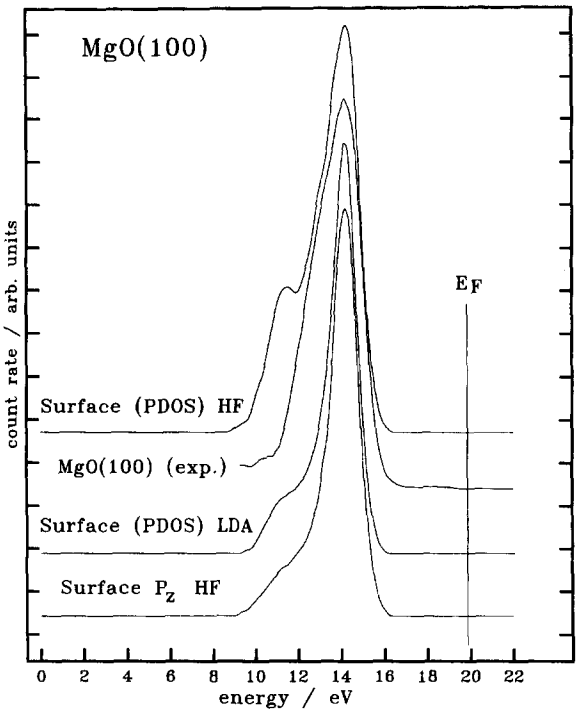

Fig. 11. Simulated MIES spectra using p_z DOS (surface p_z HF) and PDOS of the top layer, simulated using HF (surface (PDOS) HF) and LDA (surface (PDOS) LDA) compared with the experimental MIES spectrum of MgO(100) (MgO(100) (exp.)).

of states were shifted in energy scale to coincide with the positions of the peak maxima. The experimental MIES spectrum displays only one peak. The simulated MIES spectrum based on the p_z DOS also shows only one distinct peak, whereas two peaks appear if one uses the top-layer PDOS. This suggests, that He* interacts mainly with the surface p_z electrons. The interaction with the p_{xy} electrons may contribute to some extent to the low kinetic energy side of the experimental O 2p peak.

5. Discussion

The results presented above demonstrate a broad qualitative agreement between theory and experiment. However, a quantitative agreement would be impossible because all three surfaces studied experimentally in this paper contain large

amounts of structural defects, and can be non-stoichiometric and slightly charged. This has not been taken into account in the highly idealized theoretical models. In fact, the extent of the agreement achieved indicates the sensitivity of the experimental techniques to these surface defects.

In particular, the qualitative difference between the UPS and MIES spectra, which is most clearly seen for the MgO(100) bulk sample in Fig. 1, can be understood on the basis of the difference between the calculated bulk DOS and the calculated p_z DOS (see Fig. 10a and b). This comparison demonstrates that the impinging He* atoms interact predominantly with the p_z orbitals of O ions of the topmost surface layer of the surface. There are at least two reasons for this. First, the p_z orbital protrudes wider into the vacuum than the p_x and p_y orbitals, which are directed along the surface. Second, Eq. (1) (used for the calculation of the transition rate) is oversimplified and does not take into account the real overlap of surface and He 1s orbitals (i.e. it contains only an exponential factor). If one were to take that into account, there would be a prefactor to the exponential which would distinguish the contribution of the p_z from that of the p_x/p_y orbitals. To understand this, we note that the He* atom has a slightly positive effective charge, since its 2s orbital is relatively diffuse and does not screen the core as the 1s orbital does. It means that the trajectory of the He* atoms will pass predominantly over surface O^{2-} ions rather than Mg^{2+} ions. This in turn means that on average, the contribution to the transition rate from the $O2p_z$ orbital should be substantially larger than that from the O $2p_x$,$2p_y$ orbitals, since the overlap of the latter with the He 1s orbital is exactly zero when the He* atom is located directly above the surface O ion.

The experimental MIES peak (see Fig. 11) is, however, considerably wider than that simulated when only the p_z DOS is taken into account. At least three reasons could be responsible for this (i) the wider peak reflects the influence of the surface roughness or the presence of surface imperfections, such as point defects, steps, kinks, etc., (ii) the wider O 2p structure is caused by the different interaction of the probe atom with the surface before and after the electron emission, (iii) the phonon broadening of MIES may be different from that for UPS due to the difference in the surface hole relaxation energy and/or the surface phonon frequencies with respect to the bulk values.

In contrast to the MgO(100) bulk data and the data for oxidized Mg(poly), the measurements for the Mg layers on Si(100) show additional features. The XPS data obtained for oxidized Mg layers (Fig. 7) show no chemical shift of O 1s as compared with the XPS data for the MgO bulk. Furthermore, no Si contributions were observed with XPS. It must therefore be concluded that the additional structures observed with MIES and UPS are due to states of oxygen atoms (ions) located on top of the surface.

UPS features similar to the additional features obtained for the Mg film (Fig. 5) have been observed by Tjeng et al. [22] but were interpreted to be due to C contamination within the MgO bulk. The XPS measurement for the MgO(100) single crystal (Fig. 2) did not show any C contamination, and the oxide layers were also checked to be free of impurities. Another possible explanation for the additional UPS/MIES structures of Figs. 5 and 6 follows from the work of Wang et al. [55] for MgO single crystal surfaces. The MgO single crystal, investigated using REM and EELS, was heated up to elevated temperature. Above 1300 K, surface steps disappear and new surface defects are created and the surface shows structural changes and roughening. With the combination of imaging and spectroscopic techniques it was shown that on top of this surface, MgO_2 patches oriented in different directions are present. These patches were shown to be highly stable at high temperature and against high gas exposure [55].

The difference between the two top spectra of Figs. 8a and 8b produces three peaks at $E_B = 4.2$, 7.9 and 11.7 eV (corresponding to the marks 1, 2, and 3 in Figs. 5 and 6) with respect to the Fermi energy, respectively. A similar structure has been reported previously for oxygen interaction with alkali layers [1,2,20]. It was shown that such a three-peak structure can be attributed to the ionization of π_g, π_u and σ_g orbitals of O_2^{2-}; their ionization leads to three peaks that are located in the region of binding energies given above [1,2,20]. In the present case the formation of O_2

complexes may proceed via the dissociative adsorption of atomic oxygen, which binds to lattice oxygen [56].

The additional spectral features beyond the valence-band maximum observed for thin films and clearly distinguishable from the MgO bulk contributions can be tentatively attributed to film imperfections such as kinks and steps. Nevertheless, the accuracy of the present techniques does not allow us to clearly detect steps, kinks and other defects which give their contribution to the spectra within or close to the main peaks. However, controlled production of defects such as adsorbed molecules, radiation induced defects and products of chemical reactions with concentration higher than 10^{-4} should be observable in MIES difference spectra. The interpretation of these difference spectra can be based on calculations of the density of states including surface defects, similarly to the calculations for the ideal MgO crystal reported in this paper.

6. Summary

The electronic structure of the (100) surface of MgO single crystals is compared with that for oxidized polycrystalline Mg surfaces and oxidized Mg layers on Si(100) using MIES, UPS and XPS. It is demonstrated that MgO(100) bulk crystals and oxidized polycrystalline Mg surfaces show similar electronic structures. Oxidized Mg films also show the same electronic structure as MgO(100) bulk crystals after mild heat treatment at 800 K. Ab initio band-structure calculations are used to calculate the density of states of the top layers and the density of states projected into the vacuum to an image plane, where the He* – surface interaction predominantly takes place. The results of these calculations are used as a basis for the numerical simulation of MIES spectra.

The calculation of MgO DOS shows that the total DOS of MgO and the DOS projected on O 2p orbitals perpendicular to the surface are different. The comparison between UPS and MIES and the calculated DOS implies He* predominantly interacts with those electrons which occupy the O 2p orbitals directed perpendicular to the surface.

Comparison of the MIES and UPS spectra and the SDOS calculated for the ideal MgO(100) surface implies that the MgO(100) bulk crystal surface treated as described above is more perfect than the surfaces of thin oxidized films on silicon. Additional spectral features observed beyond the valence-band maximum indicate the presence of surface defects.

The spectra of oxidized Mg layers on Si(100) with thicknesses greater than 100 Å suggest the presence of O_2^{2-} complexes on the surface, which we tentatively attribute to the dissociative adsorption of oxygen binding to lattice oxygen.

Acknowledgements

Financial support of this work by the Deutsche Forschungsgemeinschaft under Grant-Nos. Ke155/24-1 and LET/113-1 and SFB 180 of the Deutsche Forschungsgemeinschaft is gratefully acknowledged. L.K. is supported by EPSRC grant GR/J37546.

References

[1] W. Maus-Friedrichs, S. Dieckhoff, M. Wehrhahn, S. Pülm and V. Kempter, Surf. Sci. 271 (1992) 113.
[2] W. Maus-Friedrichs, S. Dieckhoff and V. Kempter, Surf. Sci. 273 (1992) 311.
[3] H. Ishii, S. Masuda and Y. Harada, Surf. Sci. 239 (1990) 220.
[4] A. Hitzke, S. Pülm, H. Müller, R. Hausmann, J. Günster, S. Dieckhoff, W. Maus-Friedrichs and V. Kempter, Surf. Sci. 291 (1993) 67.
[5] S. Pülm, A. Hitzke, J. Günster, H. Müller and V. Kempter, Rad. Eff. Def. Sol. 128 (1994) 151.
[6] S. Dieckhoff, H. Müller, W. Maus-Friedrichs, H. Brenten and V. Kempter, Surf. Sci. 279 (1992) 233.
[7] S. Pülm, A. Hitzke, J. Günster, W. Maus-Friedrichs and V. Kempter, Surf. Sci. 325 (1995) 75.
[8] T. Harada, M. Asano and Y. Mizutani, J. Cryst. Growth 116 (1992) 243.
[9] Y.C. Lee, P. Tong and P.A. Montano, Surf. Sci. 181 (1987) 559.
[10] H. Onishi, C. Egawa, T. Aruga and Y. Iwsawa, Surf. Sci. 191 (1987) 479.
[11] F. Didier and J. Jupille, Surf. Sci. 307–309 (1994) 587.

[12] M.A. Karolewski and R.G. Cavell, Surf. Sci. 271 (1992) 128.
[13] J. Lahtinen, J. Vaari, A. Talo, A. Vehanen and P. Hautojärvi, Surf. Sci. 245 (1991) 244.
[14] R. Sum, H.P. Lang and H.-J. Güntherodt, Physica C 242 (1995) 177.
[15] R.A. McKee, F.J. Walker, E.D. Specht, J.G.E. Jellison, L.A. Boatner and J.H. Harding, Phys. Rev. Lett. 72 (1994) 2741.
[16] J.H. Lunsford, Agnew. Chem. Int. Ed. Engl. 34 (1995) 1570.
[17] W. Maus-Friedrichs, M. Wehrhahn, S. Dieckhoff and V. Kempter, Surf. Sci. 237 (1990) 257.
[18] W. Maus-Friedrichs, S. Dieckhoff and V. Kempter, Surf. Sci. 249 (1991) 149.
[19] J. Lee, C. Hanrahan, J. Arias, F. Bozso, R.M. Martin and H. Metiu, Phys. Rev. Lett. 54 (1985) 1440.
[20] B. Woratschek, W. Sesselmann, J. Küppers, G. Ertl and H. Haberland, Phys. Rev. Lett. 55 (1985) 611.
[21] A.G. Borisov, D. Teillet-Billy and J.P. Gauyacq, Surf. Sci. 284 (1993) 337.
[22] L.H. Tjeng, A.R. Vos and G.A. Sawatzky, Surf. Sci. 235 (1990) 269.
[23] M. Grass, J. Braun and G. Borstel, Surf. Sci. 334 (1995) 215.
[24] P.A. Zeijlmans van Emmichhoven, P.A.A.F. Wouters and A. Niehaus, Surf. Sci. 195 (1988) 115.
[25] P. Eeken, J.M. Fluit, A. Niehaus and I. Urazgil'din, Surf. Sci. 273 (1992) 160.
[26] W. Maus-Friedrichs and V. Kempter, Surf. Sci. Rep., submitted for publication.
[27] H. Brenten, H. Müller, A. Niehaus and V. Kempter, Surf. Sci. 278 (1992) 183.
[28] G. Ertl and J Küppers, Low Energy Electrons and Surface Chemistry, 2nd ed. (VCH, Weinheim, 1985).
[29] A. Arnau and P. Echenique, Phys. Rev. B 38 (1988) 10897.
[30] M.W. Cole Phys. Rev. B 2 (1970) 4239.
[31] J. Reissland, The Physics of Phonons (Wiley, New York, 1973).
[32] C. Pisani, R. Dovesi and C. Roetti, Hartree–Fock Ab-initio Treatment of Crystalline Systems, Lecture Notes in Chemistry (Springer, Heidelberg, 1988).
[33] M. Causá, R. Dovesi, C. Pisani and C. Roetti, Phys. Rev. B 33 (1986) 1308.
[34] R. Dovesi, C. Pisani, C. Roetti, M. Causá and V.R. Saunders, CRYSTAL-88, QCPE program No. 577 (Bloomington, Indiana, 1989).
[35] M. Causá, R. Dovesi, C. Pisani and C. Roetti, Surf. Sci. 175 (1986) 551.
[36] M. Causá, R. Dovesi, E. Kotomin and C. Pisani J. Phys. C 20 (1987) 4983 and 4991.
[37] A. Gibson, R. Haydock and J.P. LaFemina, J. Vac. Sci. Technol. A 10 (1992) 2361.
[38] W. Langel and M. Parrinello, Phys. Rev. Lett. 73 (1994) 504.
[39] S. Pugh and M.J. Gillan, Surf. Sci. 320 (1994) 331.
[40] A. Schamehorn, N.M. Harrison and M.I. McCarthy, J. Chem. Phys. 1010 (1994) 1547.
[41] U. Schönberger and F. Aryasetiawan, Phys. Rev. B, submitted for publication.
[42] M.C. Payne, M.P. Teter, D.C. Allan, T.A. Arias and J.D. Joannopoulos, Rev. Mod. Phys. 64 (1992) 1045.
[43] L.N. Kantorovich, J.M. Holender and M.J. Gillan, Surf. Sci.. 343 (1995) 221.
[44] L.J. Clarke, I. Stich and M.C. Payne, Comp. Phys. Commun. 72 (1992) 14.
[45] M. Iwan and C. Kunz, Phys. Lett. A 60 (1977) 345.
[46] J.J. Mackham, Rev. Mod. Phys. 31 (1959) 956.
[47] A.L. Shluger, E.N. Heifets, J.D. Gale and C.R.A. Catlow, J. Phys.: Condens. Matter 4 (1992) 5711.
[48] A. De Vita, M.J. Gillan, J.S. Liu, M.C. Payne, I. Stich and L.J. Clarke, Phys. Rev. B 46 (1992) 12964.
[49] A. Hitzke, J. Günster, J. Kolaczkiewicz and V. Kempter, Surf. Sci. 318 (1994) 139.
[50] M. Cotter, S. Campbell, R.G. Egdell and W.C. Mackrodt, Surf. Sci. 197 (1988) 208.
[51] J.C. Fuggle, Surf. Sci. 69 (1977) 581.
[52] W.C. Price, in: Electron Spectroscopy: Theory, Techniques and Applications, Vol. I, Eds. C.R. Brundle and A.D. Baker (Academic Press, London, 1977) p. 151.
[53] A.M. Shikin, G.V. Prudnikova, V.K. Adamchuk, S.L. Molodtsov, A. Guitiérrez, D. Vandré and G. Kaindl, Surf. Sci. 269/270 (1992) 1060.
[54] Y.-N. Xu and W.Y. Ching, Phys. Rev. B 43 (1991) 4461.
[55] Z.L. Wang, J. Benthley, E.A. Kenik, L.L. Horton and R.A. McKee, Surf. Sci. 273 (1992) 88.
[56] L.N. Kantorovich, M.J. Gillan, J.A. White, J. Chem. Faraday Trans. II (1996), in press.